Article

Cell Reports

Stromal-Initiated Changes in the Bone Promote Metastatic Niche Development

Graphical Abstract

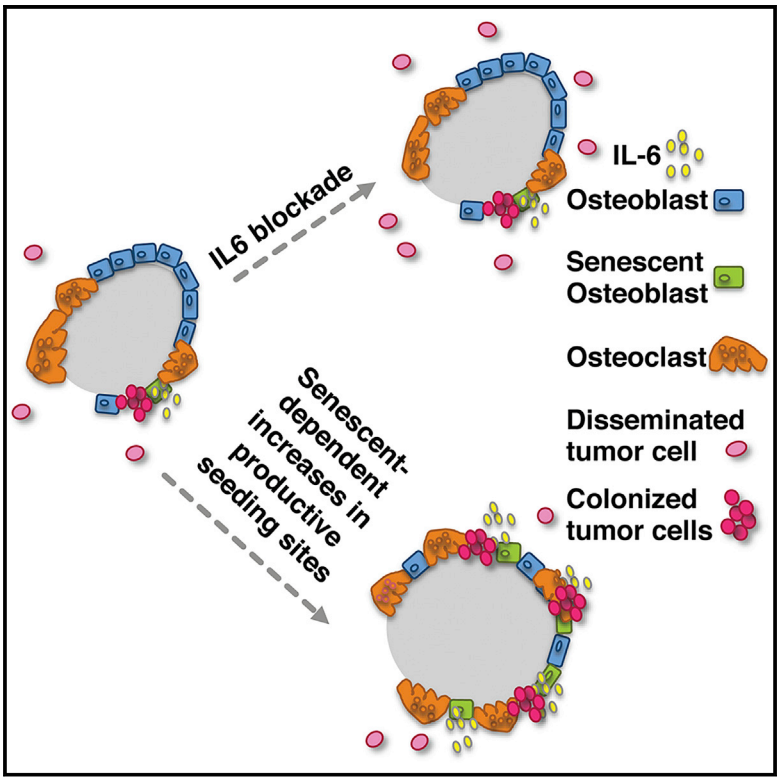

Authors

Xianmin Luo, Yujie Fu, Andrew J. Loza, ..., Roberta Faccio, Gregory D. Longmore, Sheila A. Stewart

Correspondence

sheila.stewart@wustl.edu

In Brief

Luo et al. show that stromal-derived changes are sufficient to increase tumor cell colonization and metastatic growth in the bone. They report that senescent osteoblasts, and, in particular, the senescence-associated secretory phenotype factor IL-6 drives localized osteoclastogenesis and tumor cell growth.

Highlights

- Stromal changes in the bone drive tumor cell seeding and growth
- IL-6-expressing stromal cells are present in human bone
- Senescent osteoblasts drive increased osteoclastogenesis and tumor cell seeding
- Senescent-derived IL-6 drives localized osteoclastogenesis and tumor cell growth

Luo et al., 2016, Cell Reports *14*, 1–11
January 5, 2016
http://dx.doi.org/10.1016/j.celrep.2015.12.016

CellPress

Please cite this article in press as: Luo et al., Stromal-Initiated Changes in the Bone Promote Metastatic Niche Development, Cell Reports (2016), http://dx.doi.org/10.1016/j.celrep.2015.12.016

Cell Reports
Article

Stromal-Initiated Changes in the Bone Promote Metastatic Niche Development

Xianmin Luo,[1,2,8] Yujie Fu,[1,2,8] Andrew J. Loza,[2,3] Bhavna Murali,[1,2] Kathleen M. Leahy,[1,2] Megan K. Ruhland,[1,2] Margery Gang,[1,2] Xinming Su,[3] Ali Zamani,[4] Yu Shi,[4] Kory J. Lavine,[3,5] David M. Ornitz,[5,6] Katherine N. Weilbaecher,[3,6] Fanxin Long,[3,4,5,6] Deborah V. Novack,[3,6,7] Roberta Faccio,[4,6] Gregory D. Longmore,[1,2,3,6] and Sheila A. Stewart[1,2,3,6,*]
[1]Department of Cell Biology and Physiology
[2]ICCE Institute
[3]Department of Medicine
[4]Department of Orthopedic Surgery
[5]Department of Developmental Biology
[6]Siteman Cancer Center
[7]Department of Pathology and Immunology
Washington University School of Medicine, St. Louis, MO 63110, USA
[8]Co-first author
*Correspondence: sheila.stewart@wustl.edu
http://dx.doi.org/10.1016/j.celrep.2015.12.016

SUMMARY

More than 85% of advanced breast cancer patients suffer from metastatic bone lesions, yet the mechanisms that facilitate these metastases remain poorly understood. Recent studies suggest that tumor-derived factors initiate changes within the tumor microenvironment to facilitate metastasis. However, whether stromal-initiated changes are sufficient to drive increased metastasis in the bone remains an open question. Thus, we developed a model to induce reactive senescent osteoblasts and found that they increased breast cancer colonization of the bone. Analysis of senescent osteoblasts revealed that they failed to mineralize bone matrix and increased local osteoclastogenesis, the latter process being driven by the senescence-associated secretory phenotype factor, IL-6. Neutralization of IL-6 was sufficient to limit senescence-induced osteoclastogenesis and tumor cell localization to bone, thereby reducing tumor burden. Together, these data suggest that a reactive stromal compartment can condition the niche, in the absence of tumor-derived signals, to facilitate metastatic tumor growth in the bone.

INTRODUCTION

Cancer is an ecological disease that emerges from a dynamic interplay between incipient tumor cells and their surrounding stromal environment (Hanahan and Weinberg, 2011). Stromal changes not only impact primary tumor development, but also convert future metastatic sites into a fertile environment (niche) that supports the survival and outgrowth of tumor cells (Psaila and Lyden, 2009; Sceneay et al., 2013 and references therein). An outstanding question that remains is what drives tumor cell seeding and growth within distal sites and can these changes be inhibited or reverted? This question has led to a persuasive body of work demonstrating that primary tumor cells can release factors systemically that mobilize bone-marrow-derived cells to distal target organs to condition the pre-metastatic site (Hiratsuka et al., 2002 and references found in Sceneay et al., 2013). In addition to soluble factors, exosomes released from primary tumor cells, hypoxia within the primary tumor, and primary tumor-driven reductions in immune surveillance can also modulate the pre-metastatic niche and increase metastasis to distal organs (Psaila and Lyden, 2009; Sceneay et al., 2012, 2013 and references therein). However, whether stromal cells naturally residing in the bone are sufficient to initiate changes that facilitate subsequent tumor cell seeding and growth in the absence of systemic signals generated from primary tumor cells has not been explored.

RESULTS

Senescent Osteoblasts Drive Increased Breast Cancer Growth in the Bone

To determine if stromal changes arising within the bone in the absence of signals emanating from a primary tumor are sufficient to foster tumor cell colonization, we turned our attention to the putative role that senescent stromal cells play in the process. Indeed, senescent fibroblasts secrete a plethora of factors (referred to as the senescence-associated secretory phenotype, SASP) that impact every step in the tumorigenic process (Coppé et al., 2008; Krtolica et al., 2001; Parrinello et al., 2005). As such, senescent cells recapitulate the activities of reactive stromal cells including cancer-associated fibroblasts (CAFs), which are known to impact cancer initiation and progression (Bavik et al., 2006; Olumi et al., 1999). Thus, we postulated that senescent cells create a pro-tumorigenic microenvironment that favors

Please cite this article in press as: Luo et al., Stromal-Initiated Changes in the Bone Promote Metastatic Niche Development, Cell Reports (2016), http://dx.doi.org/10.1016/j.celrep.2015.12.016

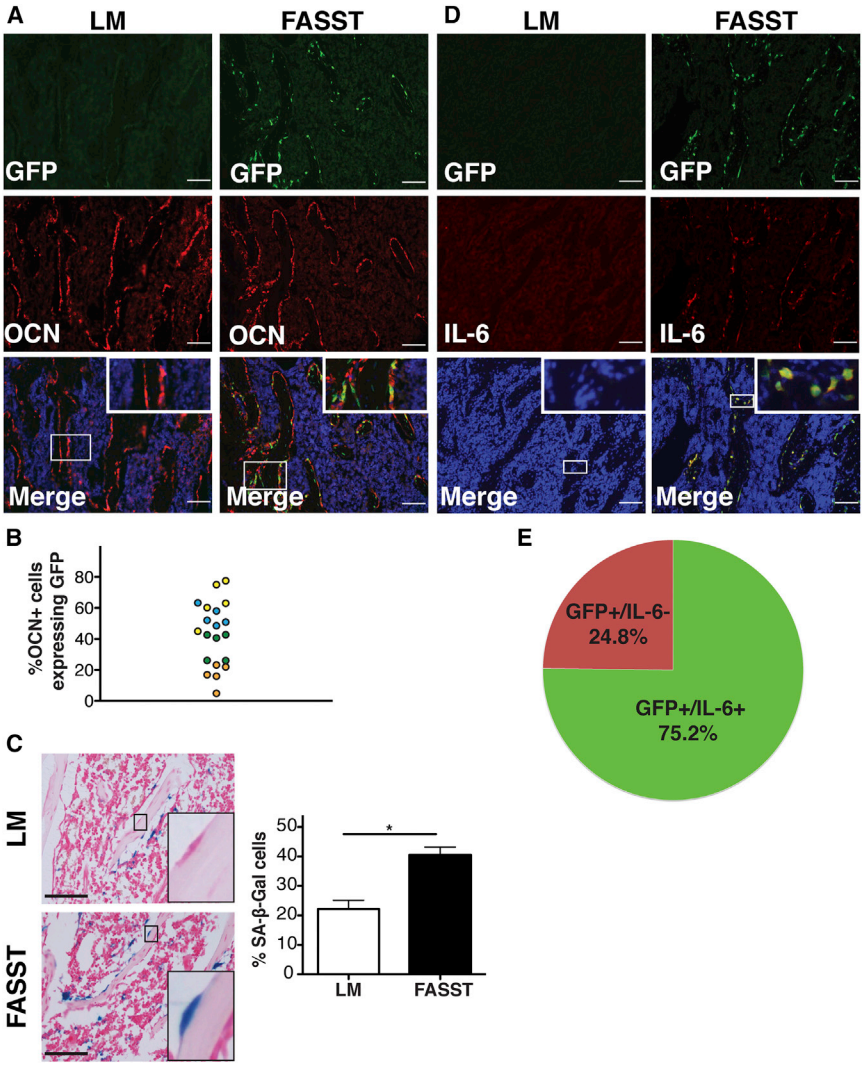

Figure 1. Transgene Activation in Osteoblasts Results in Senescence and SASP Expression

(A) Characterization of transgene activation in FASST mice. Representative immunofluorescence (IF) staining of frozen bone sections obtained from littermate (LM) control or FASST mice was performed with anti-GFP (green) and anti-osteocalcin (OCN) (red) antibodies. IF staining revealed mosaic activation with variable penetrance of the $p27^{Kip1}$ transgene (GFP^+) within OCN (+) osteoblasts (see Figure S1A). Scale bar, 100 μm; magnification 10×; inset, 20× (n = 4).

(B) Quantification of transgene activation (GFP^+) in five bone sections from four different FASST mice shows a wide variation in transgene activation. GFP-positive counts from the same mouse are coded as a single color.

(C) Representative SA-β-Gal staining in FASST versus littermate control bone sections. Quantification of SA-β-Gal staining in littermate control (LM) or FASST mice. Senescent bone-lining cells are denoted by a black arrowhead. Data are presented as a percentage of total bone-lining cells. Scale bar, 100 μm (n = 3) (*SEM, $p < 0.05$, two-tailed, Student's t test).

(D) Representative staining of IL-6 (red) SASP expression in the bones of FASST mice revealed robust activation in GFP^+ (green), senescent osteoblasts. No GFP expression was observed in the littermate (LM) mice, and no significant IL-6 expression was noted in the LM controls. Scale bar, 100 μm, magnification 10×; inset, 40× (n = 4). Secondary antibody panel with existing LM and FASST IL-6 stains can be found in Figure S1B for reference.

(E) Quantification of IL-6 expression in GFP^+ osteoblasts from bone sections of FASST mice (n = 4 mice, five bone sections each). IL-6 was expressed in ~75% of GFP-positive cells, while ~25% of GFP-positive cells had no detectable IL-6 expression.

the seeding and/or outgrowth of tumor cells and that this could occur independent of a distantly located primary tumor. To test this, we developed a conditional mouse model that allowed us to spatially and temporally control senescence induction within the mesenchymal compartment. In doing so, we hypothesized that osteoblasts, like closely related fibroblasts, undergo a senescence response that echoes that previously observed in the latter cell type. Our "FASST" (fibroblasts accelerate stromal-supported tumorigenesis) model uses a stromal-specific, estrogen-responsive Cre recombinase (Cre-ER^{T2}) to create senescent osteoblasts in mice by inducing expression of the cell-cycle inhibitor, $p27^{Kip1}$. We chose to use $p27^{Kip1}$ in our model because it faithfully recapitulated the senescent phenotype observed in human cells. Indeed, expression of $p27^{Kip1}$ is sufficient to induce senescence (Alexander and Hinds, 2001) and robust pro-tumorigenic SASP expression in fibroblasts from these mice (unpublished data). Thus, $p27^{Kip1}$ is an important tool that we have utilized to recapitulate the physiology observed in human tissue. To restrict expression to the mesenchymal compartment, mice carrying the Cre-ER^{T2} transgene driven by the pro-alpha 2(I)collagen promoter (Zheng et al., 2002) were mated to mice that conditionally express $p27^{Kip1}$ and a lineage tracing IRES GFP allele from the ROSA26 locus (ROSAlox-stop-lox-$p27^{Kip1}$IRESGFP) (Lavine et al., 2008). Cre recombinase was activated in mice 4 weeks of age and GFP expression and induction of senescence markers were monitored within the bone. To control for any unanticipated effects of tamoxifen, all mice (Cre^+ and Cre^-) received tamoxifen. Following Cre activation, we observed mosaic induction of the $p27^{Kip1}$ transgene (GFP^+ cells) within osteoblasts in murine bones (Figure 1A) with variable penetrance. Indeed, in four animals we found that 17%–64% of osteocalcin (OCN)-positive osteoblasts expressed the $p27^{Kip1}$ transgene (Figures 1B and S1A).

Having established that transgene activation occurred in osteoblasts (Figures 1A and 1B), we stained bone sections from FASST mice or littermate controls for senescence associated β-galactosidase (SA-β-Gal). $p27^{Kip1}$ transgene activation led to a mosaic yet significant induction of senescence within the

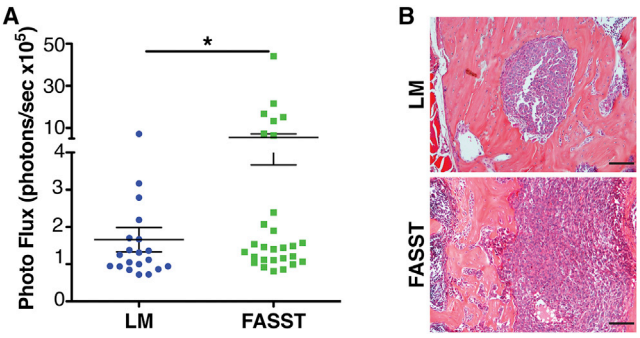

Figure 2. Senescent Stromal Cells Increase Bone Metastasis

(A) FASST mice display increased bone tumor burden. Isogenic breast cancer, NT2.5luc cells were introduced into littermate control (LM) or FASST mice by left intracardiac injection (IC). Four weeks later, mice were sacrificed, and their leg bones were imaged ex vivo. Significantly higher tumor burden was observed in FASST mice compared to littermate controls ($n > 20$). SEM, $^*p < 0.05$, unpaired Student's t test with Welch's correction. Importantly, the distribution of tumor burdens corresponded with the variable activation of senescence noted in FASST mice.

(B) Tumor morphology was assessed in littermate control (LM) versus FASST mice. Tumors in bone sections were stained with H&E, and no gross morphological differences were noted. Scale bar, 100 μm.

FASST bone (Figure 1C). Importantly, the increase in SA-β-Gal-positive cells was limited to bone-lining cells whose location suggested that they were osteoblasts (inset in Figure 1C). To determine if the activation of senescence occurred in GFP^+ osteoblasts, we co-stained bone sections from FASST mice for GFP and interleukin-6 (IL-6), a well-characterized SASP factor readily expressed in senescent human and mouse fibroblasts (Coppé et al., 2008, 2010). While lower expression of IL-6 was noted in the littermate control animals, we found that 75.2% of GFP-positive cells expressed increased levels of IL-6 in FASST bones (Figures 1D, 1E, S1B, and S1C). Hence, in this respect the osteoblasts recapitulated the well-documented senescence behavior of fibroblasts.

Breast cancer cells frequently metastasize to the bone (Coleman and Rubens, 1987); thus, we next asked if the presence of senescent osteoblasts were sufficient to support tumor cell recruitment and growth. Because spontaneous models of breast cancer metastasis to the bone do not form overt lesions, we utilized intracardiac (IC) injection to assess the impact of senescent osteoblasts on tumor cell seeding and metastatic tumor burden within the bone. Isogenic NT2.5 murine breast cancer cells (Reilly et al., 2000) stably expressing firefly luciferase (NT2.5luc) were IC injected into FASST mice or littermate controls. Given the small number of total senescent cells present in the bones of our animals and our goal to determine how senescent stromal cells impact tumor cell colonization and growth, we chose to inject only 10,000 tumor cells, which resulted in a low tumor cell burden in bones. Four weeks after injection, mice were sacrificed and tumor burden was measured in the femur and tibia bones by ex vivo bioluminescent imaging. Strikingly, there was significantly higher tumor burden in bones obtained from FASST mice compared to littermate controls (Figures 2A and 2B). While we cannot access the degree of GFP activation at endpoint in our mice because the vast majority of GFP^+ cells are no longer detectable (Figures S1D–S1F), these data are inline with the variable degree of senescence activation we observe in our model. Indeed, as we anticipated, given the variable penetrance of transgene activation in our model, analyses of tumor burdens in individual animals revealed a similar distribution when compared to the degree of GFP activation in FASST mice (Figures 1B and S1A). Together, these data suggest stochastic accumulation of senescent osteoblasts in the bone is sufficient to create a hospitable niche in the absence of signals from primary tumors.

Senescent Osteoblasts Increase Osteoclastogenesis

To establish how senescent osteoblasts increase bone metastasis, we next isolated osteoblasts (OCN-positive cells) (Figure S2A) from untreated FASST mice and analyzed how senescence impacted their function. To induce senescence in vitro, we treated FASST osteoblasts ex vivo with tamoxifen. In contrast to TAM treatment of non-Cre-ER^{T2} expressing osteoblasts (Figure S2B) and transgenic osteoblasts treated with vehicle alone, tamoxifen treatment of transgenic osteoblasts induced an enlarged, flattened, senescence-like morphology and growth arrest (Figures 3A and S2C). As expected, growth arrest correlated with robust SA-β-Gal staining and a significant increase in the well-characterized SASP factor IL-6 in tamoxifen-treated FASST osteoblasts, relative to vehicle-treated osteoblasts (Figures 3A, S2D, and S2E). SASP is characterized by expression of a wide variety of inflammatory cytokines, growth factors, and extracellular matrix remodeling enzymes. While each of these categories is expressed in cells undergoing senescence, the exact factors vary depending on the cell of origin and the tissue under scrutiny (Coppé et al., 2008; Kuilman et al., 2008; Rodier and Campisi, 2011; Ruhland et al., 2015). Because cell-cycle inhibitors including p16IN4a and p21 do not induce SASP (Coppé et al., 2011), we wanted to ensure that $p27^{Kip1}$induced SASP. Analysis of our senescent osteoblasts revealed that in addition to IL-6, sFRP, and Notch3 were robustly induced (Figure S2E). Importantly, we found that bleomycin treatment, which can activate premature stress induced senescence (SIPS), also led to increased expression of IL-6, sFRP, and Notch3 (Figure S2F). Further, analysis of murine fibroblasts ectopically expressing $p27^{Kip1}$ revealed that they too underwent robust senescence as evidenced by SA-β-Gal expression and expressed numerous inflammatory cytokines consistent with SASP described in other fibroblasts (unpublished data). Given the individual factors that contribute to the SASP is dependent on the cell of origin, our data indicated that $p27^{Kip1}$ expression is sufficient to induce senescence and SASP expression in osteoblasts.

To determine how senescence affected osteoblast function, we first examined expression of several osteoblast markers that are indicative of osteogenic function. When grown in osteogenic medium (OM), senescent osteoblasts displayed reduced levels of ALP mRNA compared to nonsenescent osteoblasts (Figure 3B). Furthermore, senescent osteoblasts displayed less ALP protein expression and alizarin red S staining than vehicle-treated osteoblasts (Figure 3C).

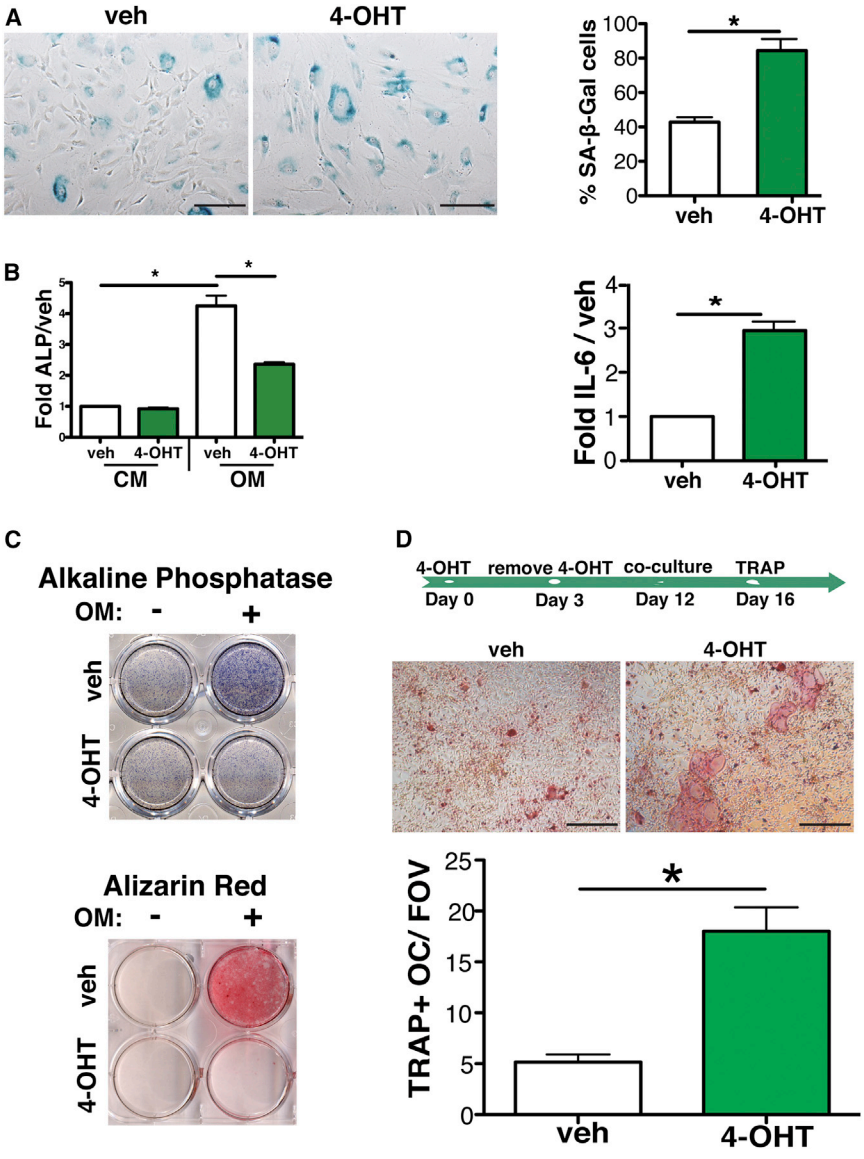

Figure 3. Senescence Abrogates Osteoblast Function and Drives Osteoclastogenesis

(A) Primary osteoblasts were obtained from the femurs of 6-week-old FASST mice. To activate the $p27^{Kip1}$ transgene and induce senescence, FASST osteoblasts were treated with 10 μM tamoxifen (4-OHT) for 3 days. SA-β-Gal staining was carried out on 4-OHT or vehicle (veh)-treated osteoblasts on day 3. 4-OHT treatment resulted in a significant increase in enlarged, flattened cells that stained positive for SA-β-Gal (blue) compared to vehicle-treated cells (upper-right panel); scale bar, 200 μm (*$p < 0.05$, two-tailed, Student's t test. one of three representative experiments is shown). The induction of the senescence associated secretory phenotype (SASP) factor IL-6 was also quantitated RT-PCR (lower-right panel). Senescent osteoblasts expressed significantly more *IL-6* mRNA compared to vehicle-treated cells (SEM, *$p < 0.05$, two-tailed, Student's t test; one of three representative experiments is shown).

(B) qRT-PCR expression of alkaline phosphatase (*ALP*) in vehicle (veh) versus 4-OHT-treated osteoblasts grown in basic culture medium (CM) versus osteogenic medium (OM). Senescent osteoblasts displayed a dramatic reduction in *ALP* mRNA levels when grown in osteogenic medium (SEM, *$p < 0.05$, two-tailed, Student's t test; one of two representative experiments is shown).

(C) ALP and alizarin red S staining in senescent versus non-senescent osteoblasts. FASST osteoblasts were treated with vehicle or 4-OHT for 3 days and then plated in basic culture medium (–) or osteogenic medium (+) for 7 or 21 additional days. On day 7 ALP expression was assessed (upper panel, one of four representative experiments is shown), and on day 21 mineralization capacity was assessed by staining with alizarin red S (lower panel, one of three representative experiments is shown). 4-OHT-treated osteoblasts displayed a robust reduction of both ALP expression and mineralization capabilities.

(D) Senescent osteoblasts increase osteoclastogenesis. As shown on the timeline, osteoblasts were treated with vehicle (veh) or 4-OHT for 3 days. 4-OHT was then removed from the culture medium, and, on day 12, after robust activation of senescence (data not shown) bone marrow macrophages were plated on non-senescent versus senescent osteoblasts, and osteoclastogenesis was determined by TRAP staining on day 16. Representative pictographs are shown; scale bar, 200 μm. TRAP-positive osteoclasts (TRAP+OC) were counted and data are displayed as TRAP+OC/field of view (TRAP+OC/FOV) (SEM, *$p < 0.05$, two-tailed, Student's t test; one of three representative experiments is shown). Because we noted that osteoclast precursor numbers were similar in co-cultures containing non-senescent and senescent osteoblasts (data not shown), this increase is due to increased osteoclast differentiation.

When we used a second conditional genetic mouse model in which senescence was induced by loss of the telomere-binding protein TRF2 (Denchi and de Lange, 2007), we observed the same phenotypes (Figures S3A–S3G). Together, these data indicate that senescent osteoblasts have significantly impaired mineralization capacity, regardless of how senescence is induced.

Increased osteoclastogenesis can contribute to tumor cell growth in the bone (Weilbaecher et al., 2011), and osteoblasts play an important role in regulating osteoclastogenesis (Long, 2012). Thus, we asked whether senescent osteoblasts increased osteoclastogenesis by co-culturing senescent or non-senescent osteoblasts with normal bone-marrow-derived macrophages. Tartrate-resistant acid phosphatase (TRAP) staining revealed that non-senescent osteoblasts produced very few osteoclasts (less than five per field of view), while senescent osteoblasts stimulated a 4-fold increase in osteoclast formation (Figure 3D). Similar results were observed when senescence was induced by loss of TRF2 (Figures S3H and S3I).

Senescent Osteoblasts Increase Tumor Cell Seeding and Metastatic Tumor Burden in the Bone

To determine if senescent osteoblasts altered the bone microenvironment, we carried out histomorphometric analysis and

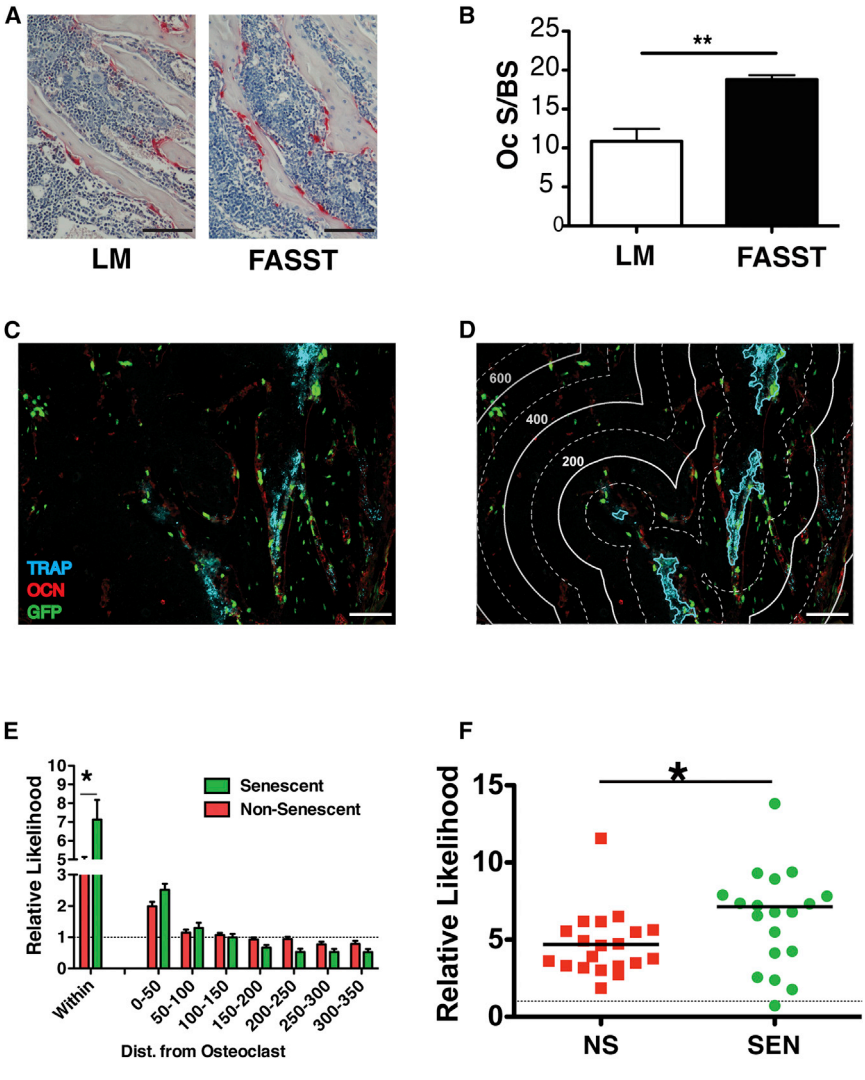

Figure 4. Senescent Osteoblasts Increase Local Osteoclastogenesis

(A) Osteoclast surface to bone surface area was assessed by TRAP staining. Representative images of bone sections from 6-week-old littermate (LM) control or FASST mice are shown and osteoclasts are indicated by red, TRAP+ staining and nuclei are counterstained with hematoxylin. For these analyses, TRAP+ cells were quantitated in the tibia near the growth plate using the Bioquant software. Scale bar, 100 μm (n = 4).

(B) Quantification of osteoclast surface area (Oc S) per bone surface (BS) was carried out on bone sections obtained from 6-week-old littermate (LM) or FASST mice (n = 4, SEM, *p < 0.05, two-tailed, Student's t test).

(C) Representative bone sections from 6-week-old FASST mice were co-stained with antibodies against GFP (green), OCN (red), and ELF97 TRAP (blue). Scale bar, 100 μm.

(D) Definition of bining distances for computational spatial analyses that were overlaid on the image presented in (C). The lines depict (1) cyan line outlines the osteoclast; (2) thick line = 200 units of distance (pixels); and (3) dashed line = 100 units of distance (pixels). Scale bar, 100 μm.

(E) Computational spatial analysis of bone sections from FASST mice show increased osteoclastogenesis within 50 units of senescent osteoblasts (within the cyan line in D). Statistical analysis of the frequency of senescent versus non-senescent osteoblasts encountering an osteoclast. Data demonstrate a higher association of osteoclasts is observed around senescent osteoblasts and this associated falls off with distance (n = 3, SEM, *p < 0.05, two-sided Wilcoxon signed-rank test).

(F) Distribution of osteoclasts "within" 50 units is shown from data in (E). As we noted in Figure 1, the distribution of osteoclasts increasing near senescent osteoblasts corresponds with the variable activation of senescence noted in FASST mice (n = 3, SEM, *p < 0.05, two-sided Wilcoxon signed-rank test).

found that senescent osteoblasts in FASST mice significantly increased the surface area of the bone covered by osteoclasts compared to total bone surface area (OC S/BS) by nearly 2-fold when compared to littermate controls (Figures 4A and 4B). Despite this increase, we failed to detect systemic evidence of bone turnover (e.g., increases in serum CTX levels or morphological bone changes by μCT, data not shown), leading us to postulate that the mosaic appearance of senescent osteoblasts in FASST mice create localized changes in bone homeostasis. This disruption would take the form of SASP-driven increases in local osteoclastogenesis and subsequent release of bone-bound latent growth factors that are known to fuel tumor cell growth in the bone (Weilbaecher et al., 2011). Further, if these local changes were restricted to areas directly surrounding senescent osteoblasts, then they would be sufficient to create focal niches that would promote tumor cell colonization. If true, we would predict that osteoclastogenesis would be enhanced around senescent osteoblasts in FASST mice.

To test this, we asked whether osteoclasts preferentially localize to areas adjacent to senescent versus non-senescent osteoblasts. Bone sections from FASST mice were stained simultaneously with antibodies against OCN to identify osteoblasts, GFP to identify senescent cells, and TRAP to identify osteoclasts (Figure 4C). We then determined the frequency of TRAP-positive osteoclasts arising in the vicinity of GFP/OCN-double-positive (senescent) osteoblasts versus GFP-negative, OCN-positive (non-senescent) osteoblasts (Figure 4D). Using statistical methods designed to analyze spatial processes (Rodan and Martin, 1981), we found as expected that osteoclasts localized near osteoblasts more frequently than chance would predict. This was demonstrated by ratios of observed to random chance being greater than 1 (dotted line on graph, Figure 4E). Strikingly, this association was significantly ($p < 0.05$) higher around GFP-positive, senescent osteoblasts (relative probability: 7.5) compared to non-senescent osteoblasts (relative probability: 4.3) when we examined osteoblasts "within" the osteoclast area (i.e., within the cyan lines, which marks

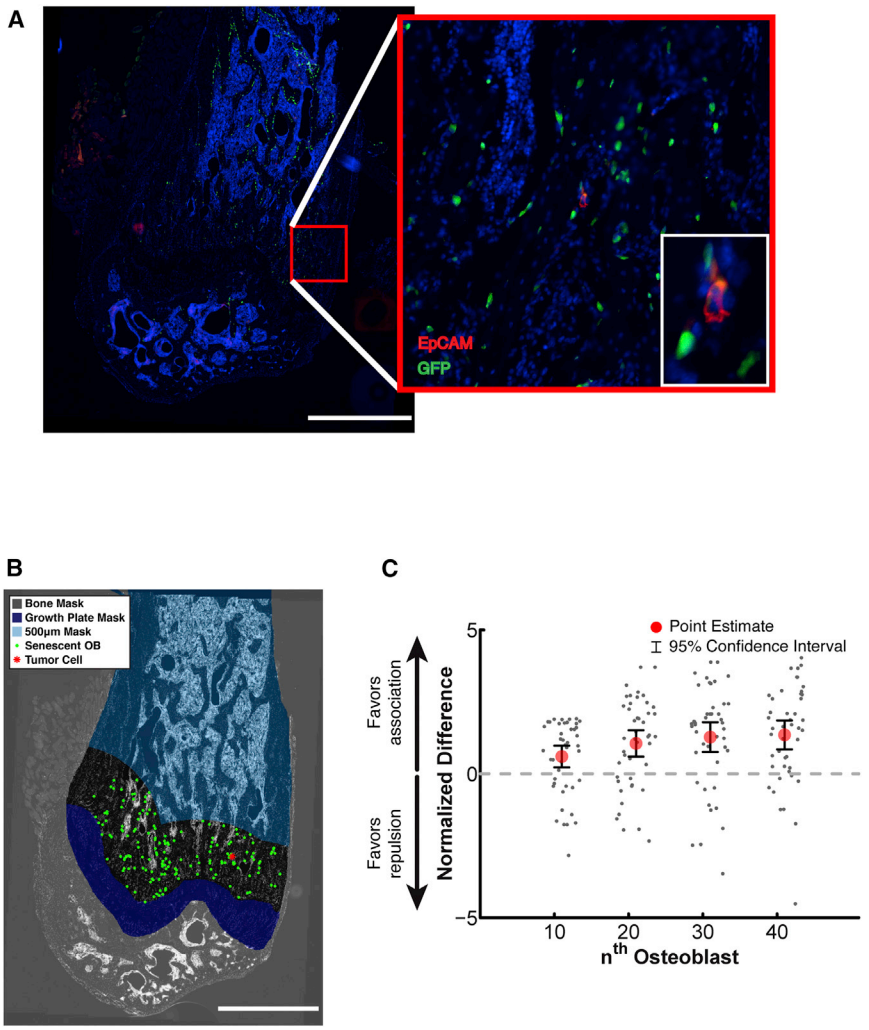

Figure 5. Senescent Osteoblasts Drive Tumor Cell Seeding

(A) Immunofluorescent staining to detect tumor cells and senescent osteoblasts in FASST mice. For these analyses, sections from the femurs of 6-week-old FASST mice were obtained 3 days after NT2.5luc cells were introduced intracardically. Femurs were completely sectioned and EpCAM staining (red) was used to identify tumor cells, and anti-GFP staining (green) was used to identify senescent osteoblasts. Representative images are shown; scale bar, 1 mm, red inset is 20×, and white inset is 60× (n = 3 femurs). Total number of tumor cells analyzed was 32, 16, and seven from bones from three different mice). Stains using a secondary antibody alone stain and FASST mice with no tumor cells can be found in Figure S4A.

(B) Computational spatial analysis of tumor cell localization. The image shown in (A) was masked as follows to determine tumor cell localization. The growth plate, which was the region of the femur where greater than 90% of tumor cells were localized, was masked to facilitate statistical analysis. Tumor cells were coded as red stars, and senescent osteoblasts were coded as green dots. Scale bar, 1 mm.

(C) The likelihood that a tumor cell (gray dots) would encounter a senescent osteoblast by chance (dotted line at 0) versus the observed frequency was calculated for each osteoblast. Osteoblast locations were sampled instead of tumor cell locations to minimize edge effects associated with tumor cells located near the border of the region of interest. Following the sampling, the mean, SD, median, and 95% confidence interval were computed. To better visualize the difference between the observed and expected distance distributions, the ratio of the observed and expected median distance functions was taken. Where this plot is greater than 1, the distance to the n^{th} senescent osteoblast from a tumor cell was larger than expected, favoring segregation of the two cell populations. Where this plot is less than 1, the distance from a tumor cell to the n^{th} nearest senescent osteoblast is smaller than expected, thus favoring association of the two populations. To allow for combination of data across multiple samples and mice, a normalized difference (also referred to as effect size) curve was computed. The difference between the observed distance and mean difference for the n^{th} nearest osteoblast was taken and normalized by sampling SD. The resulting curve provides a measure of how many SDs away from the random mean the observed results lie. To allow the graph to show positive numbers for association, the negative of the normalized difference is plotted. p values are found in Figure S5.

the border of the osteoclast, Figure 4F), indicating the increased presence of osteoclasts around GFP-positive senescent osteoblasts in vivo.

Next, we wondered whether senescent osteoblasts would also create a favorable niche for tumor cell seeding, thereby explaining the increased tumor growth observed in the bones of FASST mice. To directly test whether tumor cells traffic to regions surrounding senescent osteoblasts (observed in Figure 4C), we injected NT2.5luc cells into FASST mice and sacrificed mice 3 days later, a time point long enough to permit localization to distant tissue sites but before overt tumors are observable. To identify NT2.5luc tumor cells, we stained bone sections of FASST mice with an antibody against EpCAM, a specific marker of epithelial cells not found in the normal bone and, as before, used an antibody against GFP to identify senescent osteoblasts (Figures 5A and S4A). We then determined whether EpCAM-positive tumor cells localized near senescent, GFP-positive osteoblasts more frequently than chance would predict. To establish the degree of tumor cell localization, we utilized a similar computational approach as described above, and the data are presented as normalized to the chance that there is association (greater than one) or repulsion (less than one). These analyses revealed that tumor cells localized around senescent osteoblasts (Figures 5B, 5C, S4A, and S5) significantly more often than would be predicted by chance. Further, this association was robust because we found that, when we excluded the trabecular bone regions from our analysis, an area where tumor cells cannot localize too, it did not impact our findings (Figure S4B). Thus, our data suggest that senescent osteoblasts locally increase tumor cell seeding and/or outgrowth.

While the mechanisms that drive cancer cells to the bone remain poorly understood, it is known that osteoblast-derived CXCL12 can attract tumor cells (Taichman et al., 2002). Analyses of senescent and non-senescent osteoblasts failed to show a difference in CXCL12 expression (data not shown), suggesting that other senescent-derived factors were responsible for the increased tumor cell seeding and growth in the bone. Our model suggests that the stochastic appearance of senescent osteoblasts in the bones of FASST mice drive local increases in osteoclastogenesis, which creates a rich pro-metastatic milieu that facilitates tumor cell seeding and/or outgrowth. Thus, we hypothesized that senescence-induced osteoclastogenesis is a main driver of tumor seeding. Because we failed to observe changes in the osteoclastogenic factors, RANKL and M-CSF (data not shown), we turned our attention to the SASP factor IL-6, which can increase osteoclast differentiation (Udagawa et al., 1995), plays an important role in metastasis (Tawara et al., 2011), and is highly upregulated in senescent osteoblasts (Figures 1D, 3A, and S3S). Indeed, many cancer cells express IL-6, while others stimulate surrounding stromal cells to secrete high levels of IL-6 that drive increases in osteoclastogenesis and tumor cell adaptation and growth in the bone (Tawara et al., 2011 and references therein).

Senescent-Derived IL-6 Drives Osteoclastogenesis and Tumor Cell Growth in the Bone

To determine if senescence-derived IL-6 was responsible for the increased osteoclastogenesis observed in FASST mice, we utilized an IL-6-neutralizing antibody. Because IL-6 is required to maintain the senescent phenotype in some settings, we first confirmed that IL-6 neutralization had no impact on the maintenance of senescence or expression of SASP factors in senescent osteoblasts (data not shown and Figures S6A–S6D). Next, we carried out an ex vivo osteoclastogenesis assay. As expected, the presence of senescent osteoblasts significantly increased the number and size of osteoclasts; however, this increase was completely abrogated in the presence of an IL-6-neutralizing antibody (Figure 6A). This finding indicated that increased osteoclastogenesis is driven by high levels of senescent-derived IL-6.

Given our in vitro findings, we next asked if neutralization of senescent-derived IL-6 reduced tumor cell colonization of the bone in FASST mice. FASST or littermate mice were treated with control immunoglobulin G (IgG) or anti-IL-6 IgG, and NT2.5luc tumor cell growth in the bone was assessed following IC injection. As expected, control IgG recapitulated the increased bone colonization and tumor cell outgrowth observed in FASST mice compared to littermate controls. In contrast, treatment with anti-IL-6 led to a striking reduction in tumor burden in the bones of FASST mice that otherwise exhibited significantly higher tumor burden than littermate controls. Given the importance of the osteoblastic niche and putative role of IL-6 in bone metastasis, it was not surprising that we also noted that IL-6 neutralization reduced tumor cell growth in control animals (reduced by 7.3-fold in control and 29.9-fold in FASST mice, $p < 0.05$, Figure 6B). This finding combined with the tumor cell seeding data (Figure 5) bolsters our hypothesis that senescent osteoblasts increase the amount of productive seeding area within the bone. In fact, control mice clearly develop tumors within the bone, indicating that they are proficient in supporting tumor cell seeding and/or outgrowth. Thus, our data suggest that the activation of senescent osteoblasts in the FASST mice increases the regions within the bone that are capable of supporting tumor cell seeding and growth.

The significant loss in tumor growth within the bone observed in FASST mice following IL-6 antibody treatment raised the important question of how neutralization of IL-6 led to reduced tumor cell growth. IL-6 is mitogenic in many settings (Schafer and Brugge, 2007 and references therein), and thus senescence-associated IL-6 could directly stimulate the growth of tumor cells. This raised the possibility that IL-6 neutralization directly impacted tumor cell growth in our model. To test this possibility, conditioned medium was isolated from non-senescent and senescent osteoblasts and was added to cultures of NT2.5luc cells. As expected, senescent osteoblast-conditioned medium stimulated the growth of NT2.5luc breast cancer cells 40-fold over the growth observed in the presence of conditioned medium obtained from non-senescent osteoblasts (Figure 6C). We next asked whether this increased growth was due to IL-6 by culturing NT2.5luc cells in senescent osteoblast-conditioned medium with an IL-6-neutralizing antibody. We found that neutralization of IL-6 had no impact on the increased growth of NT2.5luc cells observed in the presence of senescent-conditioned medium, indicating that the stimulation of NT2.5luc cell growth by senescent-conditioned medium occurs independently of IL-6 (Figure 6C). Thus, while senescent osteoblasts can directly stimulate tumor cell growth, possibly adding to the observed eventual increased tumor burden, IL-6 does not directly contribute to this increased growth.

Because we failed to show that senescence-derived IL-6 directly stimulated tumor cell growth, we postulated that instead it played a critical role in senescent-driven increases in local osteoclastogenesis that promoted tumor cell seeding. Thus, we next asked if IL-6 neutralization limited the increased osteoclastogenesis we observed near senescent versus non-senescent osteoblasts. To address this possibility, littermate or FASST mice were treated with control IgG or a neutralizing IL-6 antibody prior to the activation of senescence. As expected, treatment with anti-IL-6 led to a significant reduction in osteoclast surface area to bone surface area in FASST mice (Figures 6D and S6E). In contrast, we did not observe a similar decrease in osteoclast surface area to bone surface when littermate control mice were treated with neutralizing IL-6 antibody (Figures 6D and S6E). Given this reduction, we next asked whether osteoclasts directly near senescent osteoblasts were reduced. As in our previous analyses (Figures 4C–4E), bone sections were stained simultaneously to identify senescent (GFP^+, OCN^+) and non-senescent (GFP^-, OCN^+) osteoblasts and $TRAP^+$ osteoclasts.

By utilizing the same statistical analyses for spatial processes as we did in Figures 4C–4E, we found that osteoclasts localized near osteoblasts more frequently than chance would predict in control IgG-treated animals (Figures 6E, upper panel). Further, this association was significantly ($p < 0.0117$) increased near senescent versus non-senescent osteoblasts. However, when mice were treated with anti-IL-6, this increased association was completely abrogated ($p = 1.0$) (Figure 6E, lower panel),

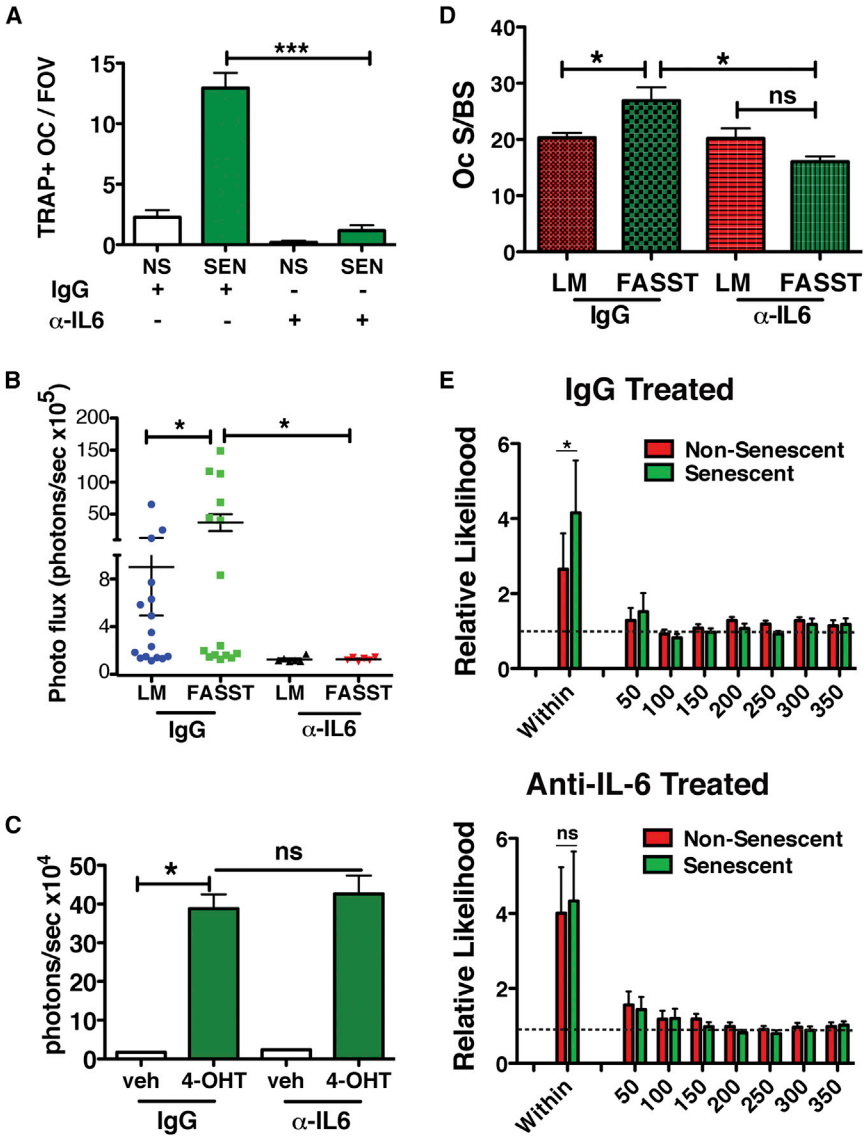

Figure 6. Senescent-Derived IL-6 Drives Increased Osteoclastogenesis and Bone Metastasis

(A) Quantification of osteoclasts following co-culture with non-senescent (NS) or senescent (SEN) osteoblasts in the presence of a control (IgG) or IL-6-neutralizing antibody (α-IL-6). Bone-marrow-derived macrophages were cultured with non-senescent or senescent osteoblasts for 4 days in the presence of 5 pg α-IL-6. The antibody was replaced every other day. TRAP staining was carried out after 4 days co-culture, and osteoclast numbers were quantitated and are displayed as TRAP-positive osteoclasts per field of view (TRAP+OC/FOV) (SEM, *p < 0.05, two-tailed, Student's t test; one of two representative experiment is shown).

(B) IL-6-neutralizing antibody reduces bone metastasis. Littermate (LM) or FASST mice were treated with 500 μg control antibody (IgG) or IL-6-neutralizing antibody (α-IL-6) on day −1 and twice weekly throughout the time course of the experiment. On day 0, NT2.5luc tumor cells were introduced by intracardiac injection. On day 28, mice were sacrificed, and tumor burden was assessed by ex vivo imaging of leg bones. Tumor burden is displayed as photon flux (photons/second) (n > 6, SEM, *p < 0.05, unpaired Student's t test).

(C) The growth of NT2.5luc cells was monitored by bioluminescent imaging in the presence of conditioned medium obtained from vehicle (veh) or 4-OHT-treated osteoblasts. Vehicle and 4-OHT-conditioned medium was treated with either a control antibody (IgG) or a neutralizing antibody against IL-6 (α-IL-6). Growth was determined by the MTT assay (SEM, *p < 0.05, two-tailed, Student's t test; one of two representative experiment is shown).

(D) Quantification of osteoclast surface area (Oc S) per bone surface (BS) was carried out on bone sections obtained from 6-week-old FASST mice treated with IgG or anti-IL-6 (n = 3 per condition, SEM, *p < 0.05, two-tailed, Student's t test).

(E) Computational spatial analysis of bone sections from FASST mice treated with IgG control antibody or anti-IL-6 show that anti-IL-6 eliminates the increased osteoclastogenesis observed locally around senescent osteoblasts. Mice were treated with IgG or anti-IL-6 2 days before receiving tamoxifen. Mice then received biweekly doses of IgG or anti-IL-6 for 2 more weeks before being sacrificed. Statistical analysis of the frequency of senescent versus non-senescent osteoblasts encountering an osteoclast in mice treated with IgG (upper panel) or anti-IL-6 (lower panel). Data demonstrate a higher association of osteoclasts is observed around senescent osteoblasts in IgG-treated mice that is absent in anti-IL-6-treated mice (n = 3, SEM, *p < 0.05 for IgG-treated mice and the p value for anti-IL-6 treated mice was 0.36 [non-significant, ns], both two-sided Wilcoxon signed-rank test).

demonstrating that IL-6 plays a central role in the increased osteoclastogenesis observed in our model.

DISCUSSION

The leading cause of cancer-related morbidity and mortality is metastasis and many solid tumor types metastasize to the bone. Indeed, nearly 80% of advanced breast cancer patients develop bone metastases (Coleman and Rubens, 1987). Growing evidence suggests that systemic effects emanating from the primary tumor prepare the metastatic niche for tumor cell arrival and survival (Psaila and Lyden, 2009; Sceneay et al., 2013). While these studies strongly support a role for the primary tumor in contributing to the development of a metastatic niche, there has been little investigation into whether local changes within the bone, independent of the actions of the primary tumor, contribute to creating a supportive niche. Our studies show that in the absence of signals emanating from a primary tumor, alterations within the bone niche are sufficient to drive seeding and growth of disseminated tumor cells.

One strength of our model is the mosaic nature of the induction of senescence, which mirrors that observed in human tissues

including the skin (Dimri et al., 1995). Also, our ability to induce the phenotype in young mice allowed us to alter the bone environment and increase tumor cell seeding within the bone and metastatic outgrowth. It is important to note that $p27^{Kip1}$ activation, while sufficient to induce senescence (Alexander and Hinds, 2001), has not been implicated in the activation of senescence in humans. In our hands, $p27^{Kip1}$ functions as a model that potently activates the SASP and thus has allowed us to test the role senescent cells and the associated SASP plays in metastatic seeding and outgrowth in the bone. Using this model, we show that tumor burdens vary in FASST mice, and this parallels the variable penetrance of senescence (GFP+ cells) activation we observe in the model. While we are unable to assess the degree of GFP activation at endpoint in our mice, our tumor cell seeding data indicate that tumor cells initially localize to areas where GF, senescent osteoblasts are present. Together these data support our hypothesis that it is the variable activation of senescence within individual bones that results in the varied tumor penetrance.

Our data further define the mechanism that drives the increased tumor cell seeding in our model. Indeed, we show that senescent-derived IL-6 drives increases in osteoclasts, and we postulate that these create active, fertile regions for disseminated tumor cells to establish metastatic outgrowths. Thus, IL-6 neutralization in our FASST mice leads to a drastic reduction in the increased osteoclast surface area to bone surface area (Oc S/BS) and reduced metastatic tumor burden in the bones. Of note, we see a similar reduction in tumors in littermate mice raising the possibility that IL-6 may function as an important metastatic driver but may not be senescence specific. Because disseminated tumor cells do seed into the bones of littermate mice, albeit at reduced levels compared to FASST mice and both are blocked by IL-6 neutralization, we postulate that the appearance of senescent osteoblasts plays a critical role in metastasis by increasing the productive and fertile seeding areas available to the tumor cells within the bone. Taken together, these data imply that in our mouse, we have increased the available fertile seeding areas within the bone by activating senescence. Thus, it may be in patients that the stochastic nature of stromal-derived alterations increases the probability of a successful seeding event within the bone.

Our findings have significant implications for how and when we think about treating patients with early versus late stage disease. Indeed, our model recapitulates the mosaic appearance of senescent cells found in human tissues (Dimri et al., 1995). This, together with our data demonstrating that the stroma is sufficient to instigate changes that favor tumor cell seeding and growth, forces us to think about targeting the stromal compartment of early-stage patients. Current clinical data indicate that breast cancer cells are present in the circulation as circulating tumor cells (CTC) and the bone as disseminated tumor cells (DTC) in many early-stage patients and that the presence of these cells predicts poor outcome (Hall et al., 2012; Lucci et al., 2012). Because patients with early-stage disease have primary lesions that may be too small to elicit systemic effects, the existence of stromal-initiated changes within the bone could support tumor CTC and/or DTC cell seeding, survival, and/or growth in the bone. Accordingly, if senescent stromal cells within the bone increase the number of cancer cells that successfully seed, it is likely that their presence will negatively impact patient outcome. Thus, this work highlights the need to understand how stromal-initiated changes alter the bone niche so that these changes can be targeted in cancer patients.

EXPERIMENTAL PROCEDURES

Mice Husbandry and Genotyping

All mice were housed in accordance with Washington University in St. Louis's Animals Studies Committee. Compound mice contained the pro-alpha 2(I) collagen gene (Col-Cre-ER^{T2} mice) (Zheng et al., 2002) and ROSA26 locus (ROSAlox-stop-lox-$p27^{Kip1}$) (Lavine et al., 2008). Primer sequences can be found in the Supplemental Experimental Procedures.

Transgene Activation and Intracardiac Injection

Four-week-old FASST female mice and control littermates were given tamoxifen (5 mg/10 g body weight) intraperitoneal (i.p.) administration twice and an additional dose of tamoxifen at 6 weeks of age. The additional tamoxifen increased the presence of GFP-positive osteoblasts (Figures S1D–S1F). 10,000 cells/50 μl PBS NT2.5 cells expressing firefly luciferase (NT2.5luc) were injected directly into the left cardiac ventricle. Bioluminescence imaging on legs was performed ex vivo 4 weeks later on an IVIS100 or IVIS Lumina (PerkinElmer; Living Image 3.2, 1- to 60-s exposures, binning 4, 8, or 16, FOV 15 cm, f/stop1, open filter) following IP injection of D-luciferin (150 mg/kg; Biosynth). For analysis, total photon flux (photons/s) was measured from a fixed region of interest using Living Image 2.6.

Bone Histomorphology and Tartrate-Resistant Acidic Phosphatase Staining

The tartrate-resistant acidic phosphatase (TRAP) staining was performed on femur or tibia bones using BioQuant software. Details of areas of interest can be found in Supplemental Experimental Procedures.

Fluorescence-based TRAP was performed using ELF97 phosphatase substrate Kit (Molecular Probes, E6601; Invitrogen) (Filgueira, 2004) followed by staining with antibodies against GFP and OCN.

Senescent-Associated β-Galactosidase and Immunofluorescence/Immunocytochemistry Staining

All SA-β-Gal and immunofluorescence staining were carried out on cryosections.

Immunofluorescence Staining

anti-GFP (1:1,000, ab13970; Abcam), anti-IL-6 (M-19) (1:50, SC-1265; Santa Cruz Biotechnology), and anti-OCN (1:50, SC-30045; Santa Cruz Biotechnology) were used. Following incubation with primary antibodies, slides were washed in PBS and incubated for 1 hr with Alexa Fluor secondary antibodies at room temperature and mounted in ProLong Gold with DAPI antifade medium.

Luciferase Labeling of NT2.5 Cells and Culture Conditions

Mouse mammary tumor cell line NT2.5 was transduced with a FUW-firefly luciferase-EGFP (FUW-FFLuc-eGFP) lentiviral construct creating NT2.5luc cells. To establish the impact of conditioned medium on NT2.5luc cell growth, conditioned medium was collected from senescent or nonsenescent FASST osteoblasts, and NT2.5luc cell growth was monitored by luciferase activity. For IL-6 neutralization experiments, NT2.5luc cells were cultured in the conditioned medium from either senescent or nonsenescent osteoblasts plus 10 pg/μl IL-6 neutralization antibody (catalog no. 554400, BD Biosciences) or IgG control (catalog no. 40041B, BioLegend). On day 3, NT2.5luc cell growth was assessed by monitoring luciferase activity.

IL-6 Neutralization in Mice

One day prior to tamoxifen injection FASST or littermate control mice received either rat anti-murine IL-6 antibody (500 μg/mouse, BioXCell) or rat anti-murine

Please cite this article in press as: Luo et al., Stromal-Initiated Changes in the Bone Promote Metastatic Niche Development, Cell Reports (2016), http://dx.doi.org/10.1016/j.celrep.2015.12.016

IgG2a control antibody (500 μg/mouse, BioXCell) via intraperitoneal (i.p.) injection. Mice continued to receive additional antibody twice a week until sacrifice.

Image Acquisition

Images were acquired using a Nikon Eclipse Ti-E microscope. Details for the osteoclast-osteoblast and senescent osteoblast-tumor spatial analysis cell can be found in Supplemental Experimental Procedures.

Cell Culture

Primary osteoblasts were grown in the culture medium (CM), ascorbic acid free alpha-MEM (catalog no. A10490, Invitrogen), containing 10% fetal bovine serum (FBS) (catalog no. SH30109.03, Thermo Scientific) and antibiotics (100 U/ml of penicillin and 100 μg/ml of streptomycin, catalog no. P0781, Sigma). To study the differentiation ability of senescent osteoblasts, cells were maintained in osteogenic medium (OM) consisting of alpha-MEM supplemented with 10% FBS, 50 μg/ml ascorbic acid (catalog no. A4544, Sigma), and 10 mM β-glycerophosphate (catalog no. G9422, Sigma). Bone marrow macrophages were cultured in alpha-MEM (catalog no. 12561, Invitrogen) containing 10% FBS (catalog no. 26140-079, Invitrogen) and 10% CMG supernatant kindly provided by D.V.N., which was made as described previously (McHugh et al., 2000). 293T cells were cultured in DMEM with 10% FBS (catalog no. F2442, Sigma) and antibiotics.

Primary Osteoblasts Isolation, Viral Transduction, and Senescence Induction

Primary osteoblasts were isolated from the long bones as described previously (Bakker and Klein-Nulend, 2012).

Primary osteoblasts isolated from the FASST p27(+/+) mice were infected with pMSCVCre-ERpuro retrovirus. To activate the p27 transgene, stably transduced osteoblasts were treated with 10 μM Tamoxifen (13258, Cayman Chemical Company) or vehicle control for 3 days and then stained for senescence-associated β-galactosidase activity as previously described (Pazolli et al., 2009). Osteoblasts were consistently maintained at 3% O_2 at 37°C.

mRNA Isolation and qRT-PCR

Total RNA was isolated from primary osteoblasts using the Ambion RiboPure RNA isolation kit (AM1924, Invitrogen) according to the manufacturer's instructions. For cDNA synthesis, 1 μg of RNA was reverse-transcribed using SuperScript II (18064-014, Invitrogen) according to the manufacturer's instructions. The qPCR was performed using a CFX96 Real-Time system (Bio-Rad) and TaqMan gene expression assays for IL-6, ALP RANKL, and OPG. GAPDH was used as the endogenous control (Invitrogen). To establish the impact of IL-6 neutralization on IL-6 expression, 10 pg/μl of an IL-6 neutralization antibody (catalog no. 554400, BD Biosciences) or IgG control (catalog no. 40041B, BioLegend) was added to the senescent osteoblasts for 4 days, and SASP expression was analyzed by RT-PCR.

Osteoblast Differentiation Assays

To assess differentiation, 1 × 10^5 osteoblasts/well were plated onto 6-well plates in culture medium (CM). The following day medium was replaced with osteogenic medium, which was refreshed every 3 days. RNA isolation and alkaline phosphatase staining was carried out on day 7, and alizarin red S staining was carried out on day 21.

Alkaline phosphatase staining was performed as previously described (Katagiri et al., 1994). For alizarin red S staining, osteoblasts were fixed in 70% ethanol for 1 hr, rinsed with water, and stained with 0.4% alizarin red S (A5533, Sigma) (pH 4.1–4.3) for 10 min at room temperature.

Bone Marrow Macrophage Isolation and Osteoblast-BMM Co-culture Assay

Bone marrow macrophage (BMM) were obtained from 6-week-old mice. For the co-culture assay, 2 × 10^4 senescent versus control osteoblasts and 1 × 10^5 BMMs/well were plated into 24-well plates with 10 nM 1,25$(OH)_2$ $VitD_3$ (D1530, Sigma) and 100 nM dexamethasone (D4902, Sigma). The cells were co-cultured for 4 days and then stained for tartrate-resistant acid phosphatase activity using the Acid Phosphatase, Leukocyte (TRAP) kit (387A, Sigma) according to the manufacturer's instructions. For IL-6 neutralization in this assay, senescent or non-senescent osteoblasts were co-cultured with BMMs, and 5 pg/μl of IL-6 neutralization antibody (catalog no. 554400, BD Biosciences) or 5 pg/μl of IgG control (catalog no. 40041B, BioLegend) was added to the medium. The antibody was replenished every other day, and mature osteoclasts formation was detected by TRAP staining on day 4.

Statistical Analyses

All statistical analyses were carried out using GraphPad prism. Numerical data are expressed as mean ± SEM. Mouse analyses were performed by Student's t test or Mann-Whitney test as indicated in the figure legends. Description of statistical analyses used in bone analysis of osteoclastogenesis and tumor localization can be found in the description of the computational approach in Experimental Procedures.

SUPPLEMENTAL INFORMATION

Supplemental Information includes Supplemental Experimental Procedures and six figures and can be found with this article online at http://dx.doi.org/10.1016/j.celrep.2015.12.016.

AUTHOR CONTRIBUTIONS

X.L., Y.F., A.J.L., B.M., K.M.L., M.K.R., M.G., X.S., A.Z., and Y.S. carried out experiments. A.J.L. provided statistical analysis and developed the spatial analyses. G.D.L., K.N.W., F.L., and R.F. supplied experimental design and data analysis. D.V.N. provided pathological analysis and experimental design input, and S.A.S. conceived of the project and analyzed data. Finally, S.A.S., X.L., and Y.F. prepared the manuscript.

ACKNOWLEDGMENTS

We thank Ben Dao, Kelly Carbery, Joshua Behlman, and Cynthia Hernandez for assistance in establishing the FASST mouse breeding colonies and Lynne Collins and Julie Prior for assistance in animal imaging. We thank Rosy Luo for assistance with statistical analysis and Mia Wallace for assistance with speed congenics. We thank Raphael Kopan and Barry Sleckman for mouse genetics advice and Michele A. Hurchla, Jingyu Xiang, Jenna Regan, Diana Zamora, Billy McManus, Yulia Ivanova, Rong Zeng, Marcus Watkins, and Roberto Civitelli for advice and assistance. We extend a special thanks to Drs. Robert Weinberg and Daniel Link and members of S.A.S.'s lab for helpful comments. We thank Dr. Elizabeth Jaffee for the kind gift of the NT2.5 cells and Drs. Denton and Benoit de Crombrugghe for the kind gift of the Col-Cre-ER^{T2} mice. We thank Drs. Denchi and de Lange for the kind gift of the conditional TRF2 mice. Financial support was provided by NIH 5 R01CA151518 (S.A.S.) and American Cancer Society Research Scholar Award (S.A.S.). The work was supported in part by the Alvin J. Siteman Cancer Research Fund at Washington University in St. Louis, MO (S.A.S.) and Siteman Cancer Center/Barnes-Jewish Hospital Foundation (S.A.S.), the Susan G. Komen Breast Cancer Foundation (S.A.S.), Washington University Center for Aging (S.A.S.), Mary Kay Ash Charitable Foundation (S.A.S.), NIH AR052705 (D.V.N.), NIH HD049808 (D.M.O.), NIH CA143868 (G.D.L.), and NIH CA097250 (K.N.W.). A.J.L. was supported by training grants T32EB018266 and T32GM007200. Histologic analysis was supported in part by the Washington University Center for Musculoskeletal Research and the NIH/National Institute of Arthritis and Musculoskeletal and Skin Diseases (NIAMS) grant AR057235. The Molecular Imaging Center and NIH P50 CA094056 (PIs Samuel Achilefu and David Piwnica-Worms) support animal imaging.

Received: June 15, 2015
Revised: October 22, 2015
Accepted: November 23, 2015
Published: December 24, 2015

REFERENCES

Alexander, K., and Hinds, P.W. (2001). Requirement for p27(KIP1) in retinoblastoma protein-mediated senescence. Mol. Cell. Biol. *21*, 3616–3631.

Bakker, A.D., and Klein-Nulend, J. (2012). Osteoblast isolation from murine calvaria and long bones. Methods Mol. Biol. *816*, 19–29.

Bavik, C., Coleman, I., Dean, J.P., Knudsen, B., Plymate, S., and Nelson, P.S. (2006). The gene expression program of prostate fibroblast senescence modulates neoplastic epithelial cell proliferation through paracrine mechanisms. Cancer Res. *66*, 794–802.

Coleman, R.E., and Rubens, R.D. (1987). The clinical course of bone metastases from breast cancer. Br. J. Cancer *55*, 61–66.

Coppé, J.P., Patil, C.K., Rodier, F., Sun, Y., Muñoz, D.P., Goldstein, J., Nelson, P.S., Desprez, P.Y., and Campisi, J. (2008). Senescence-associated secretory phenotypes reveal cell-nonautonomous functions of oncogenic RAS and the p53 tumor suppressor. PLoS Biol. *6*, 2853–2868.

Coppé, J.P., Desprez, P.Y., Krtolica, A., and Campisi, J. (2010). The senescence-associated secretory phenotype: the dark side of tumor suppression. Annu. Rev. Pathol. *5*, 99–118.

Coppé, J.P., Rodier, F., Patil, C.K., Freund, A., Desprez, P.Y., and Campisi, J. (2011). Tumor suppressor and aging biomarker p16(INK4a) induces cellular senescence without the associated inflammatory secretory phenotype. J. Biol. Chem. *286*, 36396–36403.

Denchi, E.L., and de Lange, T. (2007). Protection of telomeres through independent control of ATM and ATR by TRF2 and POT1. Nature *448*, 1068–1071.

Dimri, G.P., Lee, X., Basile, G., Acosta, M., Scott, G., Roskelley, C., Medrano, E.E., Linskens, M., Rubelj, I., Pereira-Smith, O., et al. (1995). A biomarker that identifies senescent human cells in culture and in aging skin in vivo. Proc. Natl. Acad. Sci. USA *92*, 9363–9367.

Filgueira, L. (2004). Fluorescence-based staining for tartrate-resistant acidic phosphatase (TRAP) in osteoclasts combined with other fluorescent dyes and protocols. J. Histochem. Cytochem. *52*, 411–414.

Hall, C., Krishnamurthy, S., Lodhi, A., Bhattacharyya, A., Anderson, A., Kuerer, H., Bedrosian, I., Singh, B., and Lucci, A. (2012). Disseminated tumor cells predict survival after neoadjuvant therapy in primary breast cancer. Cancer *118*, 342–348.

Hanahan, D., and Weinberg, R.A. (2011). Hallmarks of cancer: the next generation. Cell *144*, 646–674.

Hiratsuka, S., Nakamura, K., Iwai, S., Murakami, M., Itoh, T., Kijima, H., Shipley, J.M., Senior, R.M., and Shibuya, M. (2002). MMP9 induction by vascular endothelial growth factor receptor-1 is involved in lung-specific metastasis. Cancer Cell *2*, 289–300.

Katagiri, T., Yamaguchi, A., Komaki, M., Abe, E., Takahashi, N., Ikeda, T., Rosen, V., Wozney, J.M., Fujisawa-Sehara, A., and Suda, T. (1994). Bone morphogenetic protein-2 converts the differentiation pathway of C2C12 myoblasts into the osteoblast lineage. J. Cell Biol. *127*, 1755–1766.

Krtolica, A., Parrinello, S., Lockett, S., Desprez, P.Y., and Campisi, J. (2001). Senescent fibroblasts promote epithelial cell growth and tumorigenesis: a link between cancer and aging. Proc. Natl. Acad. Sci. USA *98*, 12072–12077.

Kuilman, T., Michaloglou, C., Vredeveld, L.C., Douma, S., van Doorn, R., Desmet, C.J., Aarden, L.A., Mooi, W.J., and Peeper, D.S. (2008). Oncogene-induced senescence relayed by an interleukin-dependent inflammatory network. Cell *133*, 1019–1031.

Lavine, K.J., Schmid, G.J., Smith, C.S., and Ornitz, D.M. (2008). Novel tool to suppress cell proliferation in vivo demonstrates that myocardial and coronary vascular growth represent distinct developmental programs. Dev. Dyn. *237*, 713–724.

Long, F. (2012). Building strong bones: molecular regulation of the osteoblast lineage. Nat. Rev. Mol. Cell Biol. *13*, 27–38.

Lucci, A., Hall, C.S., Lodhi, A.K., Bhattacharyya, A., Anderson, A.E., Xiao, L., Bedrosian, I., Kuerer, H.M., and Krishnamurthy, S. (2012). Circulating tumour cells in non-metastatic breast cancer: a prospective study. Lancet Oncol. *13*, 688–695.

McHugh, K.P., Hodivala-Dilke, K., Zheng, M.H., Namba, N., Lam, J., Novack, D., Feng, X., Ross, F.P., Hynes, R.O., and Teitelbaum, S.L. (2000). Mice lacking beta3 integrins are osteosclerotic because of dysfunctional osteoclasts. J. Clin. Invest. *105*, 433–440.

Olumi, A.F., Grossfeld, G.D., Hayward, S.W., Carroll, P.R., Tlsty, T.D., and Cunha, G.R. (1999). Carcinoma-associated fibroblasts direct tumor progression of initiated human prostatic epithelium. Cancer Res. *59*, 5002–5011.

Parrinello, S., Coppe, J.P., Krtolica, A., and Campisi, J. (2005). Stromal-epithelial interactions in aging and cancer: senescent fibroblasts alter epithelial cell differentiation. J. Cell Sci. *118*, 485–496.

Pazolli, E., Luo, X., Brehm, S., Carbery, K., Chung, J.J., Prior, J.L., Doherty, J., Demehri, S., Salavaggione, L., Piwnica-Worms, D., and Stewart, S.A. (2009). Senescent stromal-derived osteopontin promotes preneoplastic cell growth. Cancer Res. *69*, 1230–1239.

Psaila, B., and Lyden, D. (2009). The metastatic niche: adapting the foreign soil. Nat. Rev. Cancer *9*, 285–293.

Reilly, R.T., Gottlieb, M.B., Ercolini, A.M., Machiels, J.P., Kane, C.E., Okoye, F.I., Muller, W.J., Dixon, K.H., and Jaffee, E.M. (2000). HER-2/neu is a tumor rejection target in tolerized HER-2/neu transgenic mice. Cancer Res. *60*, 3569–3576.

Rodan, G.A., and Martin, T.J. (1981). Role of osteoblasts in hormonal control of bone resorption–a hypothesis. Calcif. Tissue Int. *33*, 349–351.

Rodier, F., and Campisi, J. (2011). Four faces of cellular senescence. J. Cell Biol. *192*, 547–556.

Ruhland, M.K., Coussens, L.M., and Stewart, S.A. (2015). Senescence and cancer: an evolving inflammatory paradox. Biochim Biophys Acta, Published online October 8, 2015. http://dx.doi.org/10.1016/j.bbcan.2015.10.001.

Sceneay, J., Chow, M.T., Chen, A., Halse, H.M., Wong, C.S.F., Andrews, D.M., Sloan, E.K., Parker, B.S., Bowtell, D.D., Smyth, M.J., et al. (2012). Primary tumor hypoxia recruits CD11b+/Ly6Cmed/Ly6G+ immune suppressor cells and compromises NK cell cytotoxicity in the premetastatic niche. Cancer Res. *72*, 3906–3911.

Sceneay, J., Smyth, M.J., and Möller, A. (2013). The pre-metastatic niche: finding common ground. Cancer Metastasis Rev. *32*, 449–464.

Schafer, Z.T., and Brugge, J.S. (2007). IL-6 involvement in epithelial cancers. J. Clin. Invest. *117*, 3660–3663.

Taichman, R.S., Cooper, C., Keller, E.T., Pienta, K.J., Taichman, N.S., and McCauley, L.K. (2002). Use of the stromal cell-derived factor-1/CXCR4 pathway in prostate cancer metastasis to bone. Cancer Res. *62*, 1832–1837.

Tawara, K., Oxford, J.T., and Jorcyk, C.L. (2011). Clinical significance of interleukin (IL)-6 in cancer metastasis to bone: potential of anti-IL-6 therapies. Cancer Manag. Res. *3*, 177–189.

Udagawa, N., Takahashi, N., Katagiri, T., Tamura, T., Wada, S., Findlay, D.M., Martin, T.J., Hirota, H., Taga, T., Kishimoto, T., and Suda, T. (1995). Interleukin (IL)-6 induction of osteoclast differentiation depends on IL-6 receptors expressed on osteoblastic cells but not on osteoclast progenitors. J. Exp. Med. *182*, 1461–1468.

Weilbaecher, K.N., Guise, T.A., and McCauley, L.K. (2011). Cancer to bone: a fatal attraction. Nat. Rev. Cancer *11*, 411–425.

Zheng, B., Zhang, Z., Black, C.M., de Crombrugghe, B., and Denton, C.P. (2002). Ligand-dependent genetic recombination in fibroblasts : a potentially powerful technique for investigating gene function in fibrosis. Am. J. Pathol. *160*, 1609–1617.